

An ultraluminous X-ray microquasar in NGC 5408?

R. Soria,¹* R. P. Fender,² D. C. Hannikainen,³ A. M. Read⁴ and I. R. Stevens⁵

¹Harvard-Smithsonian Center for Astrophysics, 60 Garden Street, Cambridge, MA 02138, USA

²School of Physics & Astronomy, University of Southampton, Southampton SO17 1BJ

³Observatory PO Box 14, 00014 University of Helsinki, Finland

⁴Department of Physics & Astronomy, University of Leicester, Leicester LE1 7RH

⁵School of Physics and Astronomy, University of Birmingham, Birmingham B15 2TT

Accepted 2006 February 28. Received 2006 February 16; in original form 2006 January 9

ABSTRACT

We studied the radio source associated with the ultraluminous X-ray source in NGC 5408 ($L_X \approx 10^{40}$ erg s⁻¹). The radio spectrum is steep (index ≈ -1), consistent with optically thin synchrotron emission, not with flat-spectrum core emission. Its flux density (≈ 0.28 mJy at 4.8 GHz, at a distance of 4.8 Mpc) was the same in the March 2000 and December 2004 observations, suggesting steady emission rather than a transient outburst. However, it is orders of magnitude higher than expected from steady jets in stellar-mass microquasar. Based on its radio flux and spectral index, we suggest that the radio source is either an unusually bright supernova remnant, or, more likely, a radio lobe powered by a jet from the black hole (BH). Moreover, there is speculative evidence that the source is marginally resolved with a radius ~ 30 pc. A faint H II region of similar size appears to coincide with the radio and X-ray sources, but its ionization mechanism remains unclear. Using a self-similar solution for the expansion of a jet-powered electron–positron plasma bubble, in the minimum-energy approximation, we show that the observed flux and (speculative) size are consistent with an average jet power $\approx 7 \times 10^{38}$ erg s⁻¹ $\sim 0.1L_X \sim 0.1L_{\text{Edd}}$, an age $\approx 10^5$ yr, a current velocity of expansion ≈ 80 km s⁻¹. We briefly discuss the importance of this source as a key to understand the balance between luminosity and jet power in accreting BHs.

Key words: black hole physics – supernova remnants – radio continuum: ISM – X-rays: binaries – X-rays: individual: NGC 5408 X-1.

1 INTRODUCTION

Ultraluminous X-ray sources (ULXs) are point-like, accreting X-ray sources with apparent isotropic luminosities \gtrsim a few 10^{39} erg s⁻¹, that is, greater than the Eddington limit of a stellar-mass black hole (BH). Their nature remains unexplained. In particular, for the large majority of ULXs, two fundamental questions remain unsolved: whether the emission is isotropic or beamed towards the observer (either as a mild geometrical beaming, or as a collimated, relativistic jet); and whether the accreting compact objects are young, perhaps formed in recent starburst episodes, or are instead old relics of a primordial stellar population.

Studying the ULX counterparts at other wavelengths may offer clues on their ages, mechanisms of formation, isotropic luminosities [through their effect on the interstellar medium (ISM)] and sources of fuel. In particular, it has recently become clear that there is a strong connection between X-ray and radio properties of accreting BHs. This connection has been successfully applied to BH X-ray

binaries in our Galaxy, providing a physical interpretation to their state transitions (Fender, Belloni & Gallo 2004). Similar studies for accreting BHs in nearby galaxies (e.g. Fender, Southwell & Tzioumis 1998) are, however, hampered by the faintness of the radio counterparts.

The ULX in the nearby ($d = 4.8$ Mpc: Karachentsev et al. 2002) dwarf starburst galaxy NGC 5408 (henceforth, X-1) is an ideal test case for our study. Its position is known to $\lesssim 0''.5$, from a series of *Chandra* observations. The source is among the brightest ULXs in the local Universe, with an isotropic X-ray luminosity $\approx 1 \times 10^{40}$ erg s⁻¹ in the 0.3–12 keV band. Always detected in an active state also by *Einstein*, *ROSAT* and *XMM-Newton*, X-1 has shown a pattern of flux variability over a few weeks or months (Kaaret et al. 2003), as well as on shorter time-scales (Soria et al. 2004), inconsistent with an X-ray supernova remnant (SNR). Thus, there is no doubt that the X-ray emission is due to accretion on to a compact object. Most importantly, it is one of the very few ULXs with a radio counterpart (Kaaret et al. 2003). The possibility that it is a background object (radio galaxy or quasar) can be ruled out due to the extremely high X-ray to optical flux ratio (Kaaret et al. 2003); a background blazar is also very unlikely, because their radio spectral

*E-mail: rsoria@cfa.harvard.edu (RS)

indices are much flatter than determined for this source (Kaaret et al. 2003, and Section 2 of this work).

Two alternative scenarios have been suggested for X-1 (Kaaret et al. 2003; Soria et al. 2004). It could be a stellar-mass microblazar (i.e. a microquasars with its relativistic jet oriented along our line of sight). In this case, its extreme brightness would be due to Doppler boosting; its radio emission would be synchrotron from the jet; its X-ray spectrum could be produced by synchrotron self-Compton or external Compton scattering of low-energy photons [including ultraviolet (UV)/optical photons from the disc or the donor star] by the relativistic jet (Georganopoulos, Aharonian & Kirk 2002; K rding, Falcke & Markoff 2002; Georganopoulos & Kazanas 2003). Alternatively, the X-ray emission could be isotropic, implying a mass $\gtrsim 100 M_{\odot}$ for the accreting BH, if the Eddington limit is not persistently violated. Applying conventional phenomenological models, the 0.3–10 keV spectrum is dominated by a rapidly varying power-law component with photon index $\Gamma \approx 2.7$, plus a non-varying soft thermal component or ‘soft excess’ ($kT \approx 0.13$ keV), often found in ULXs.

We re-observed the system in the radio, with a more extended spectral coverage (four instead of two bands), to measure its spectral index, and to determine whether there has been a long-term variation in the radio flux compared with the previous observations in March 2000 (Stevens, Forbes & Norris 2002). Using these new results, we want to determine whether the radio emission is coming directly from the accreting BH (for example, from a relativistic jet) or is instead only spatially associated with it (for example, it may come from an underlying SNR). In either case, we will obtain important information on the geometry of emission or on the immediate environment of the ULX. More generally, we want to determine whether the associated radio and X-ray emissions in X-1 are consistent with the correlations found in Galactic BH binaries, as a function of spectral state (Fender, Belloni & Gallo 2004).

2 ATCA RADIO STUDY

We observed NGC 5408 on 2004 December 9–11, with the Australia Telescope Compact Array (ATCA), located at Narrabri, New South Wales. The array was in the 6-km configuration. Two sets of observations were carried out: simultaneously at 1.344 GHz (20 cm) and 2.638 GHz (13 cm); and simultaneously at 4.840 GHz (6 cm) and 6.208 GHz (5 cm),¹ with a continuum bandwidth of 128 MHz. Observations of the target galaxy were alternated with those of the primary flux calibrator PKS B1934–638, and of the secondary phase calibrator PKS B1320–446. In total, we had about 13 h spent on source for each of the two configurations.

The data were processed and analysed using the MIRIAD package (Sault, Teuben & Wright 1995). Images were cleaned with 1000 iterations of gain 0.1. The clearest image of the radio counterpart to the ULX is available at 4.8 GHz (Fig. 1), in which the source is clearly resolved from the nearby starburst and has a flux density of 0.28 ± 0.07 mJy (consistent with Kaaret et al. 2003). The best-fitting radio coordinates of the source associated with the ULX, obtained from the peak of the emission in the 4.8-GHz map, is RA = $14^{\text{h}}03^{\text{m}}19^{\text{s}}.65$, Dec. = $-41^{\circ}22'58''.7$ with an error $\approx 0''.3$. This is consistent (within $0''.2$) with the X-ray position of the ULX (RA = $14^{\text{h}}03^{\text{m}}19^{\text{s}}.63$, Dec. = $-41^{\circ}22'58''.7$; Kaaret et al. 2003), which we

¹ We chose to observe at 5 cm, rather than the more standard 3 cm, because of severe weather conditions, which made it impossible to preserve phase coherence at higher frequencies.

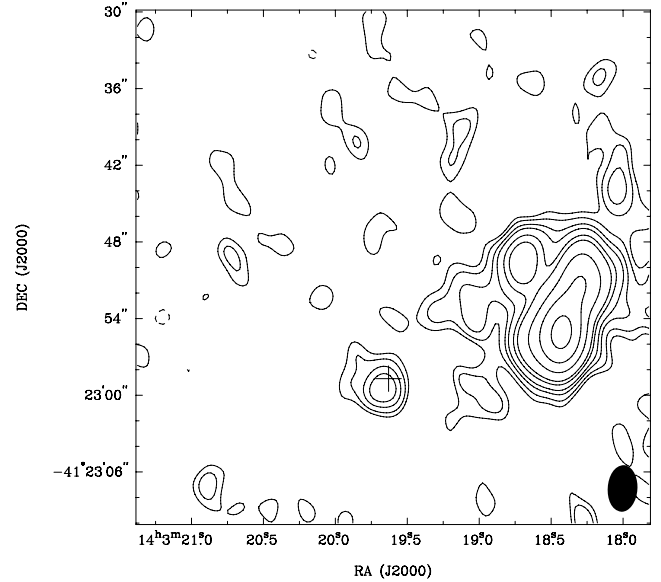


Figure 1. The ATCA radio map at 4.8 GHz (6 cm). The X-ray position of the ULX is marked with a cross. The integrated 4.8-GHz flux from the ULX counterpart is ≈ 0.28 mJy.

also re-checked by analysing the *Chandra* observations available in the public archive.

From the images at other wavelengths, it was immediately apparent that the relative faintness of the target, combined with its proximity to the starburst region, was resulting in strong uncertainties in the measured flux density. In order to quantify this, we have varied the beam size at each frequency by adjusting Briggs’ ROBUST parameter between -2 and $+2$, corresponding to a smooth transition from uniform (highest angular resolution, lowest signal-to-noise ratio) to natural (lowest angular resolution, highest signal-to-noise ratio). For each resultant map, we have fit a point-source model, with the coordinates fixed to those established from the 4.8 GHz map. The variation of the apparent source flux as a function of beam size, for each frequency, is presented in Fig. 2. Beam size is clearly a strong effect at 1.3 and 2.4 GHz, less so at 4.8 GHz and has no significant effect at 6.2 GHz: hence, it is hard to confidently

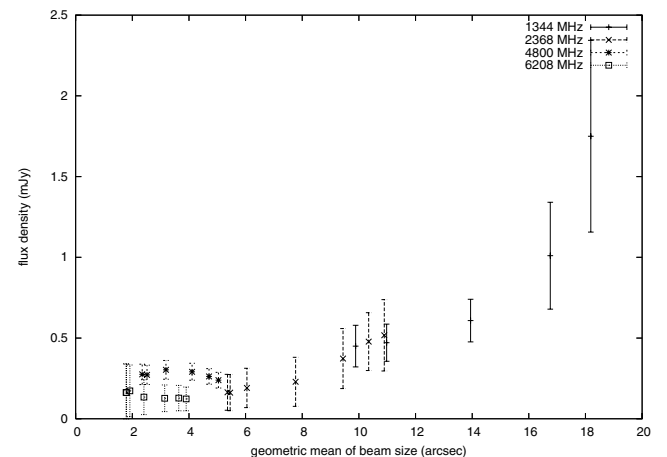


Figure 2. Changes in the apparent source flux as a function of beam size, in the four radio bands. At low frequencies, the source is contaminated by extended emission from nearby star-forming regions. See Section 2 for details.

ascribe a well-measured flux density to the radio counterpart of the ULX, particularly at low frequencies. A 4.8-GHz radio flux density of (0.28 ± 0.07) mJy corresponds to a radio luminosity of $(3.7 \pm 0.9) \times 10^{34}$ erg s $^{-1}$. As noted above, the measured flux is consistent with the 4.8-GHz flux inferred from the March 2000 ATCA observations (Stevens et al. 2002; Kaaret et al. 2003), suggesting that the source has not varied significantly between the two epochs.

Between the highest two frequencies, the marginal detection at 6.2 GHz (in the naturally weighted maps, the point-source fit at the position fixed from the 4.8-GHz image is 0.12 ± 0.07 mJy) suggests at face value a very steep spectrum with spectral index $\alpha_R \leq -3$.² This is an extreme value for synchrotron emission: it may suggest that the break due to ageing of the electron populations is located between those two bands. We will discuss – and essentially rule out – this possibility in Section 3.6. Alternatively, it may be taken as a hint that we are starting to resolve the source at those higher frequencies, which would imply a characteristic size $\approx 3 \times 2$ arcsec², or $\approx 50 \times 70$ pc² at the assumed distance of NGC 5408. At lower frequencies, contamination by the flux from the starburst starts to dominate. This makes determining the radio spectrum associated with the ULX problematic.

In another approach to estimate the radio spectral index at the ULX position and in the surrounding region, we obtained radio images of the field by combining the 1.3- and 2.4-GHz maps (Fig. 3, left-hand panel) and the 4.8- and 6.2-GHz maps (Fig. 3, right-hand panel). The radio source associated with the ULX clearly stands out as a discrete (and possibly resolved) blob in the combined high-frequency map, with hints of emission trailing back to the nearby bright starburst region. In the low-frequency map, there is clearly radio emission at the ULX location, apparently as the end of an elongated region emanating from the starburst complex, but our spatial resolution is not sufficient for a more detailed analysis. We then took the ratio of the low- and high-frequency maps (Fig. 4). From this, we note that the bright starburst region is clearly strongly resolved out on its outer edges, which is why the spectral index in these regions appears steeper than -2 . Instead, both the core of the starburst region and the site of the ULX are not resolved out, and have spectral indices ≈ -1 between these two combined bands. So, while a qualitative approach based on the measured flux densities at four frequencies for the ULX is problematic, there is strong evidence that the radio emission at the site of the ULX has a steep spectral index, consistent with optically thin synchrotron emission, and in agreement with the March 2000 observations (Kaaret et al. 2003). Incidentally, the flux-ratio map also suggests that the radio emission in the core of the starburst region is dominated by SNRs (steep spectrum) rather than free-free emission from H II regions (flat spectrum).

3 DISCUSSION

3.1 Steady jet in a low/hard state?

Given that the evidence for a spatially resolved radio source is still only marginal, we will consider both the scenario of a point-like source (core emission) and that of an extended source. We start by considering the possibility that the radio emission is directly

² Throughout this paper, the spectral index is defined such that $F_\nu \sim \nu^\alpha$, and we use α_R or α_X to avoid confusion between the radio and X-ray spectral slopes. Using the notation more commonly adopted in X-ray studies, the X-ray photon index $\Gamma \equiv -\alpha_X + 1$.

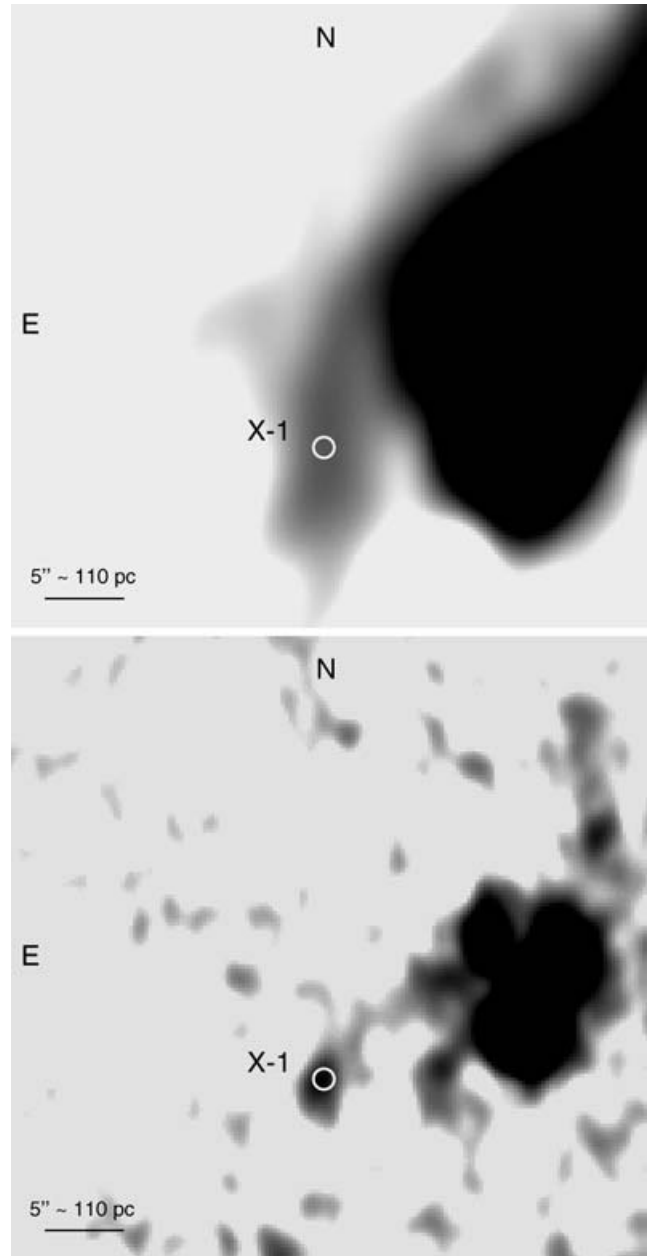


Figure 3. Top panel: radio map of the field obtained by combining the 1.3- and 2.4-GHz data. The *Chandra* position of the ULX is marked with an error circle of radius 0.6 arcsec. Bottom panel: radio image obtained by combining the 4.8- and 6.2-GHz maps.

produced by the accreting BH, on spatial scales comparable to the accretion disc. Radio emission from Galactic BH X-ray binaries is known to occur – with different physical properties – in two spectral states: the ‘low/hard’ state (LHS) and the ‘very-high’ state (VHS) (Fender et al. 2004).

The LHS is characterized by a steady jet, with moderately low bulk Lorentz factor ($\gamma \lesssim 1.4$; Gallo, Fender & Pooley 2003; Fender et al. 2004). In a steady state, there is a ‘Fundamental Plane’ correlation between radio luminosity, X-ray luminosity and BH mass (Falcke, Körding & Markoff 2004; see also Merloni, Heinz & di Matteo 2003; Fender et al. 2004), of the form

$$L_X \propto L_R^m M_{\text{BH}}^{\alpha_X - m\alpha_R}, \quad (1)$$

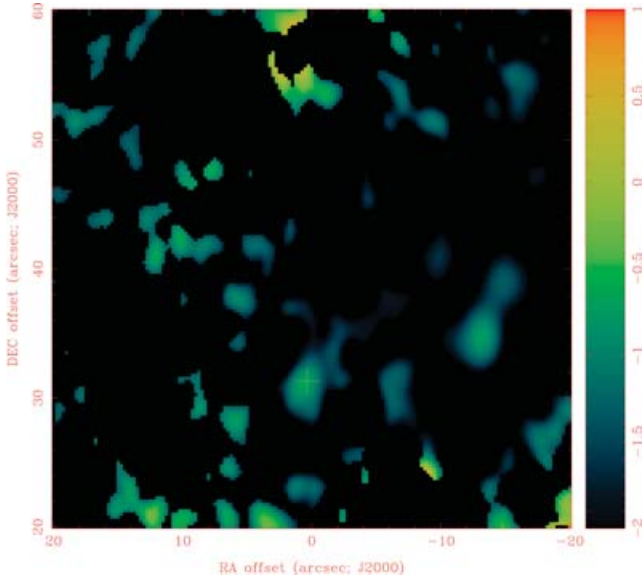


Figure 4. Ratio of the high- and low-frequency maps, showing that the ULX counterpart has a steep spectral index ($\alpha_R \approx -1$). The scale and orientation of the image is the same as in Fig. 3; the ULX position is marked with a cross.

where

$$m = \frac{(17/12) - (2/3)\alpha_X}{(17/12) - (2/3)\alpha_R} \quad (2)$$

(Markoff et al. 2003). Taking this relation at face value – or, equivalently, using the empirical relation $\log L_R = 0.60 \log L_X + 0.78 \log M + 7.33$ (Merloni et al. 2003) – we would infer a BH mass $\sim 10^4 M_\odot$, well in excess of any estimates of other ULX masses, including the strong intermediate-mass BH candidate in M 82 (Strohmayer & Mushotzky 2003; Fiorito & Titarchuk 2004).

However, there are at least two reasons why we rule out this result as unphysical. First, the observed radio spectral index ($\alpha_R \approx -1$) is too steep to be consistent with an LHS steady jet, which is typically optically thick (core-dominated), with flat or slightly inverted radio spectrum (Fender et al. 2004). Secondly, the X-ray spectrum (Soria et al. 2004) is itself inconsistent with an LHS. The X-ray spectrum in an LHS is dominated by a power law of spectral index $\alpha_X \approx -0.5$ (i.e. photon index $\Gamma \approx 1.5$ as more commonly defined in X-ray literature). Instead, the observed X-ray spectrum of X-1 is much steeper (softer), with $\alpha_X = -1.7 \pm 0.2$ (i.e. $\Gamma \approx 2.7$). We conclude

that the radio emission is not consistent with a steady jet from an accreting BH in the LHS.

3.2 Flaring jet in the very-high state?

The X-ray spectrum (Soria et al. 2004) is consistent with the classical VHS of Galactic X-ray binaries, also called the ‘steep power-law’ state, using the revised state classification of McClintock & Remillard (2003). Steady jets with a flat or inverted radio spectrum are sometimes observed in the ‘hard’ subdivision of the VHS: this can be considered a high-luminosity extension of the LHS discussed (and ruled out) in Section 3.1. Stronger radio flares are observed in Galactic sources at the transition between the ‘hard’ and ‘soft’ subdivisions, as the sources become softer and cross the ‘jet line’ (see fig. 7 of Fender et al. 2004). These flares are interpreted as discrete relativistic radio ejections, with a higher bulk Lorentz factor than in an LHS jet ($\gamma \sim$ a few: Gallo et al. 2003). One explanation for the steep-spectrum radio emission is optically thin synchrotron, from internal shocks in the jet, consequence of the sudden increase in the Lorentz factor during the state transition (Fender et al. 2004).

Well-known examples of Galactic BH binaries with a radio-flaring behaviour in their VHS include GRS 1915+105, GRO J1655–40 and XTE J1550–564 (Table 1). If moved to the distance of NGC 5408, even at their peaks, they would appear two to three orders of magnitude fainter than the radio counterpart of X-1. Moreover, the radio to X-ray flux ratio is at least an order of magnitude higher in X-1, compared to those Galactic sources (Fig. 5). Again, one might suggest that the enhanced radio luminosity, and radio-to-X-ray flux ratio are due to a much higher BH mass in X-1.

However, even if X-1 is interpreted (based on its X-ray properties) as a BH binary in the VHS, quantitative comparisons with radio-flaring Galactic BHs are highly problematic. The VHS is a short-lived transient state, and a major ejection is a brief (rise time $\lesssim 1$ d), sporadic event (once every few months or years), as the source undergoes a hard to soft transition, associated with a change in the accretion disc inner radius. In our case, the radio flux was the same on the two occasions in which the source was observed, almost 5-yr apart. Catching X-1 during a major flare once would be a remarkable coincidence; observing it twice in exactly the same state would be too unlikely. Moreover, there is no evidence of any X-ray spectral-state transitions over a series of *Chandra* and *XMM-Newton* observations spanning the years 2001–04. Hence, it is more likely that the observed radio emission is a persistent feature of this source.

The only marginally viable alternative is that the source is persistently in the VHS, oscillating in a ‘dip-flare’ cycle like GRS

Table 1. Parameters for the brightest radio outbursts in Galactic BH candidates. All jet events listed here occurred in the very-high state, with both the jet power and the X-ray luminosity estimated to be \sim Eddington. Data from Fender et al. (2004); other references are F99: Fender et al. (1999), B02: Brocksopp et al. (2002), B06: Brocksopp et al. (in preparation), H00: Hjellming et al. (2000), O01: Orosz et al. (2001), HR95: Hjellming & Rupen (1995) and W02: Wu et al. (2002).

Source	M_{BH} (M_\odot)	Date (MJD)	Peak 5-GHz flux (mJy at 4.8 Mpc)	L_J/L_{Edd}	L_X/L_{Edd}	Reference
GRS 1915+105 (flr)	14	50 750	1.7×10^{-3}	0.6	1.1	F99
GRS 1915+105 (osc)	14	50 750	2.6×10^{-4}	0.05	1.1	F99
XTE J1748–288	7	50 980	1.7×10^{-3}	1.9	0.1	B06
V4641 Sgr	9	51 437	1.2×10^{-3}	0.8	4	H00, O01
GRO J1655–40	7	49 580	1.1×10^{-3}	1.0	0.1	HR95
XTE J1550–564	9	51 077	2.0×10^{-4}	0.3	0.5	W02
XTE J1859+226	7	51 467	7.8×10^{-5}	0.2	0.2	B02

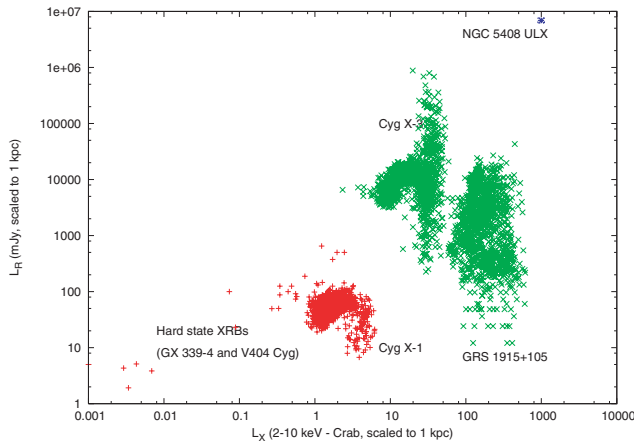


Figure 5. Comparison between the X-ray and radio fluxes from NGC 5408 X-1 and from some of the brightest Galactic microquasars, either in the LHS (steady jet) or in the VHS (flaring). In the on-line version of this plot, LHS data points are plotted in red, VHS in green. NGC 5408 X-1 is a few orders of magnitude brighter, especially in the radio band. However, we argue that the comparison is not relevant, because the radio emission from the X-1 location comes either from an underlying SNR, or, much more likely, from a radio lobe.

1915+105, crossing the jet line back and forth in the process (Fender et al. 1999; Fender & Belloni 2004, and references therein); this state is characterized by moderate X-ray and radio flaring on time-scales of a few hundred seconds. Repeated flaring on similar time-scales is indeed observed in the power-law component of the X-ray spectrum of X-1 (Soria et al. 2004). Finding the source in that same dip-flare cycle in 2000 and 2004 (and in a similar X-ray spectral state consistent with the VHS in all observations between those two epochs) could perhaps suggest that this ULX has a different spectral-state behaviour than classical Galactic X-ray binaries.

The peak radio flux density of GRS 1915+105 in the oscillatory state is three orders of magnitude lower than the radio flux of X-1, scaled to the same distance (Table 1). Taken at face value, the intensity of the radio emission from X-1 in 2000 and 2004 make this ULX very peculiar, in comparison with typical Galactic BH X-ray binary, in which the radio emission is believed to come from a compact jet (Fig. 5). However, we must also consider the possibility that the radio source associated to X-1 is enhanced by Doppler boosting, as we will discuss in Section 3.3.

3.3 Relativistically beamed emission?

Relativistic Doppler boosting is a possible mechanism to reconcile the brightness of X-1 with those of Galactic BHs, as originally suggested by Kaaret et al. (2003). The amplification of the rest-frame emission due to Doppler boosting $\sim \delta^{k-\alpha_R}$, where $\delta = \gamma^{-1} (1 - \beta \cos \theta)^{-1}$ and $2 \leq k \leq 3$ depending on whether it is a continuous jet or sporadic ejections. Having already ruled out (Section 3.2) both a steady jet in the LHS and a single major flare, we only need to estimate the Doppler boosting required for a persistent dip-flare cycle. In GRS 1915+105, the Lorentz factor γ in this state is $\gtrsim 2$ and perhaps as high as 5 (Fender et al. 2004); at a viewing angle $\approx 65^\circ$, the observed 5-GHz flux is ≈ 50 mJy at 11 kpc, corresponding to ≈ 0.3 μ Jy at 4.8 Mpc. To enhance this value by a factor of $\approx 10^3$, a viewing angle $\theta \lesssim 20^\circ$ (for $k = 3$) or $\theta \lesssim 15^\circ$ (for $k = 2$) is required, for a source identical to GRS 1915+105 and $\gamma = 5$. Allowing for an intrinsic radio luminosity an order of magnitude stronger than in GRS 1915+105 (justified by the fact that the apparent X-ray

luminosity is also a factor of 10 higher), only $\theta \lesssim 30^\circ$ (for $k = 3$) or $\theta \lesssim 25^\circ$ (for $k = 2$) are required. As an aside, we note that in order to allow for persistent dip-flare ejections with Lorentz factors ≈ 5 , the microquasar would have to reside in a large low-density bubble, otherwise the jet–ISM interaction would rapidly reduce the jet speed.

For the X-ray emission, strong beaming is disfavoured by the presence of a soft, non-variable thermal component at $kT_{bb} = 0.13 \pm 0.01$ keV, with unabsorbed luminosity $\approx 3 \times 10^{39}$ erg s $^{-1}$ in the 0.3–1 keV band (Soria et al. 2004). It is still unclear whether this soft component, typical of many ULXs (Miller, Fabian & Miller 2004; Feng & Kaaret 2005), comes from the accretion disc or from a downscattering corona or outflow (e.g. King & Pounds 2003; Laming & Titarchuk 2004), or perhaps from a combination of reflection and absorption (Gierlinski & Done 2004; Chevallier et al. 2006; Crummy et al. 2006); but in any case, it is difficult to reconcile with relativistically beamed emission. Thus, it is more likely that at least the soft component of the X-ray emission is isotropic, requiring a BH with a mass $\gtrsim 100 M_\odot$ to satisfy the Eddington limit. It is possible, instead, that the power-law component is beamed, for example, produced by inverse-Compton scattering of disc photons by the jet (e.g. Bosch-Ramon, Romero & Paredes 2005; Georganopoulos et al. 2002).

We conclude that Doppler boosting by a relativistic jet can in principle explain the observed radio flux and is not inconsistent with the X-ray properties. However, we consider this scenario somewhat contrived because it relies on the source spending most of its time in a ‘persistent’ VHS with steep-spectrum dip-flare oscillations over many years. This is unlike the typical spectral-state behaviour of Galactic X-ray binaries and microquasars; no other sources with the same behaviour have been found yet. The other difficulty is that we have at least speculative evidence to believe that the radio source is extended over $\gtrsim 30$ pc (Section 2), which would rule out point-like core emission.

3.4 Supernova remnant?

In all the scenarios discussed – and in most cases ruled out – so far, the radio emission would be coming from the innermost region around the BH, and would be directly related to its current state of accretion. We will now consider the possibility that the emission comes, instead, from a larger region in the ISM around the BH.

The association with free–free radio emission from a star-forming region was already ruled out (Kaaret et al. 2003) due to the observed steep spectrum, inconsistent with thermal bremsstrahlung. A steep optically thin synchrotron spectrum would instead be consistent with an underlying shell-like SNR: remnants in this class have typical radio spectral indices $-1 \lesssim \alpha_R \lesssim -0.4$. On the other hand, we can rule out filled-centre (plerionic, or pulsar-wind-nebula) SNRs – such as the Crab – because their spectral indices are much flatter ($-0.3 \lesssim \alpha_R \lesssim -0.1$; e.g. Weiler & Panagia 1978). Our observed index $\alpha_R \approx -1$ would be among the steepest, but not unique. For example, at least three, and possibly five of the 14 shell-like SNR candidates in NGC 300 have a spectral index $\lesssim -1$ (Pannuti et al. 2000); three of the 15 shell-like SNR candidates in NGC 6946 have an index between -1.4 and -1.0 (Hyman et al. 2000); two of the 53 SNRs in M 33 (including both plerion and shell-like SNRs) have an index ≈ -1.1 (Duric et al. 1995).

The radio flux of our source in NGC 5408 (≈ 0.28 mJy at 4.8 GHz) would also be among the highest for SNRs in nearby galaxies, but not unique. The brightest radio SNRs in NGC 300 would only reach a flux density ≈ 0.06 mJy at the distance of NGC 5408. However,

six of the 15 radio SNR candidates in NGC 6946 would have a 5-GHz flux $\gtrsim 0.2$ mJy (Hyman et al. 2000); the brightest SNR in that galaxy would have a flux ≈ 0.5 mJy. All five of the candidate SNRs in NGC 4258 (Hyman et al. 2001) are also brighter, with fluxes ≈ 0.6 – 0.7 mJy at the distance of X-1. In NGC 7793, four of the five brightest radio SNRs would have fluxes ≈ 0.08 – 0.12 mJy at the distance of NGC 5408 (Pannuti et al. 2002); however, the brightest candidate SNR in that galaxy, NGC 7793–S26, has a spectral index $\alpha_R = -0.9 \pm 0.2$ and would have a 5-GHz flux ≈ 0.6 mJy. The brightest shell-like SNR in our Galaxy, Cas A, would be seen with a 5-GHz flux of ≈ 0.3 mJy (Reynoso & Goss 2002) and a diameter of ≈ 0.2 arcsec.

One explanation for such exceptionally bright SNRs is that they are produced by very massive stars with strong winds; hence, the explosion occurred in a dense circumstellar environment (Dunne, Gruendl & Chu 2000). Alternatively, the remnants may be the result of multiple SN explosions, perhaps inside a star cluster (Pannuti et al. 2002). Either scenario would be consistent with a direct physical association between the SNR and the process of formation of the ULX X-1. In addition, a relatively young age may play a role. In summary, a bright shell-like SNR would be consistent with the measured fluxes and spectral index, would explain why the flux has been approximately the same between 2000 and 2004, and would be a natural candidate for the formation of the ULX. If, as we speculate, the radio source in NGC 5408 is marginally resolved with a diameter ~ 50 – 70 pc, we can apply the purely empirical correlation between age and diameter, found in Galactic SNRs (Xu, Zhang & Han 2005): we obtain an age $\gtrsim 10^4$ yr, with a best-fitting age $\approx 10^5$ yr (but with a large scatter). Thus, the source would be too large to be a very young or historical SNR (like Cas A). In Sections 3.5 and 3.6, we will try to find more stringent tests to the SNR scenario, based on the minimum-energy condition, and suggest an alternative explanation.

3.5 H α emission: SNR or X-ray photoionization?

The SNR scenario was initially rejected (Kaaret et al. 2003) because there appeared to be no evidence of optical emission lines at the X-1 position [upper limit of $\approx 7 \times 10^{-15}$ erg s $^{-1}$ cm $^{-2}$ derived for H α by Kaaret et al. (2003), from a broad-band *Hubble Space Telescope* (*HST*)/WFPC2 image in the F606W filter]. Although the ULX appears to be well separated from the starburst region, in broad-band optical images (e.g. the *B*-band *Subaru* image in Fig. 6, left-hand panel; and the *HST*/WFPC2 image in Kaaret et al. 2003), a narrow-band H α image (Fig. 6, right-hand panel) shows instead that most of the galaxy is filled by a tangled web of H II filaments and knots. For this study, we downloaded and analysed public-archive H α and R-continuum images taken from the European Southern Observatory (ESO) 3.6-m telescope (EFOSC camera) by M. Pakull and L. Mirioni.

In particular, an H α -emitting knot is visible at the ULX position (Fig. 7) (as noted in Mirioni 2003; Pakull & Mirioni 2003): it has a slightly elongated shape, with a size of $\approx 50 \times 70$ pc, matching the upper limit (and possibly the true size) of the radio-emitting blob. We checked that the slight displacement between the H α knot and the radio and X-ray positions is within the error in the astrometry of the optical image (~ 1 arcsec); therefore, the H α , radio and X-ray emission are consistent with being coincident. The H α knot is connected to the main starburst region through a network of filaments and cavities (Fig. 7). We estimate a flux $f_{H\alpha} = (5 \pm 2) \times 10^{-16}$ erg cm $^{-2}$ s $^{-1}$ from that knot, corresponding to a luminosity $L_{H\alpha} = (1.5 \pm 0.4) \times 10^{36}$ erg s $^{-1}$ in the line (or $\approx 5 \times 10^{47}$ H α photons s $^{-1}$),

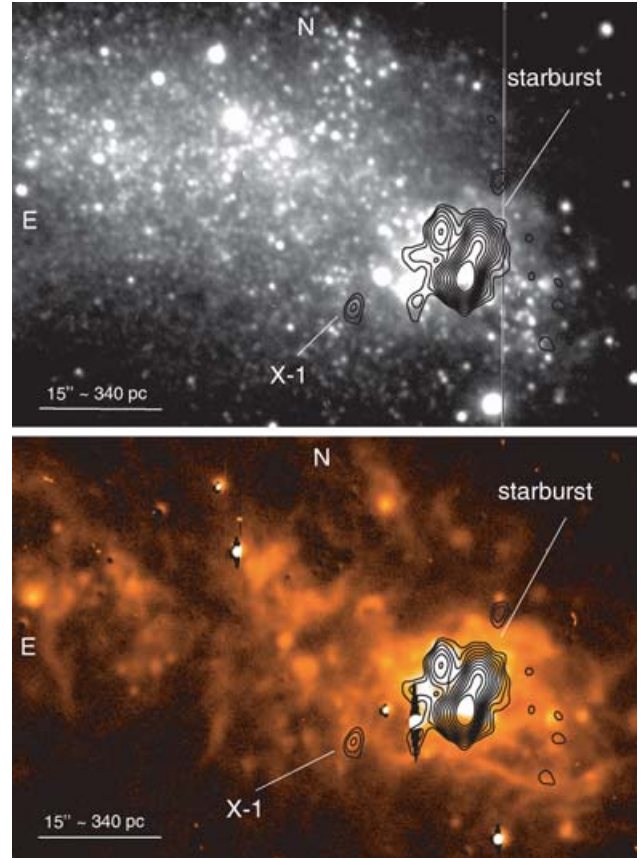


Figure 6. The ATCA radio flux density contours at 4.8 GHz, overplotted on a *B* image from *Subaru* (left-hand panel) and an H α image from the ESO 3.6-m telescope (right-hand panel), on the same spatial scale.

that is, $\sim 10^{-3}$ times the total H α emission from NGC 5408. The peak surface brightness $S_{H\alpha} \approx 1.5 \times 10^{-16}$ erg cm $^{-2}$ s $^{-1}$ arcsec $^{-2}$.

If the H α line emission is due to recombination, its estimated luminosity requires a flux of ~ 1 – 2×10^{48} ionizing photons s $^{-1}$ intercepted by the nebula (Osterbrock 1989; cf. also similar calculations for other photo-ionized nebulae in Pakull & Angebault 1986; Soria et al. 2005). This is a relatively modest requirement. Continuum *Subaru* and *HST* images show three massive stars near the peak of the radio and H α emission, with absolute *B* magnitudes ≈ -6 and bluish colours, $B - V \lesssim 0$ (Kaaret et al. 2003; Copperwheat et al., in preparation). They are consistent with main-sequence O stars, or, more likely, blue supergiants. Three such stars with initial masses $\sim 20 M_{\odot}$ would provide enough ionizing photons to explain the H α emission (Schaerer & de Koter 1997; Sternberg, Hoffmann & Pauldrach 2003). As a consistency check, the size of a Strömgren sphere at a characteristic temperature $T \approx 10^4$ K is $R_S \approx 30 Q_{48}^{1/3} n_H^{-2/3}$ pc, where Q_{48} is the photoionizing flux in units of 10^{48} photons s $^{-1}$ and n_H is the hydrogen number density in units of 1 cm $^{-3}$. This is in agreement with the observed size of the H II region at the ULX position.³

³ Note that the thermal (free-free) radio emission associated with a photoionized H II region of such size and luminosity is ≈ 500 times fainter than the non-thermal emission measured at the ULX position (Dickel, Harten & Gull 1983; Lazendic, Dickel & Jones 2003). Hence, the thermal contribution is absolutely negligible in our case, and does not affect our estimate of the radio spectral index.

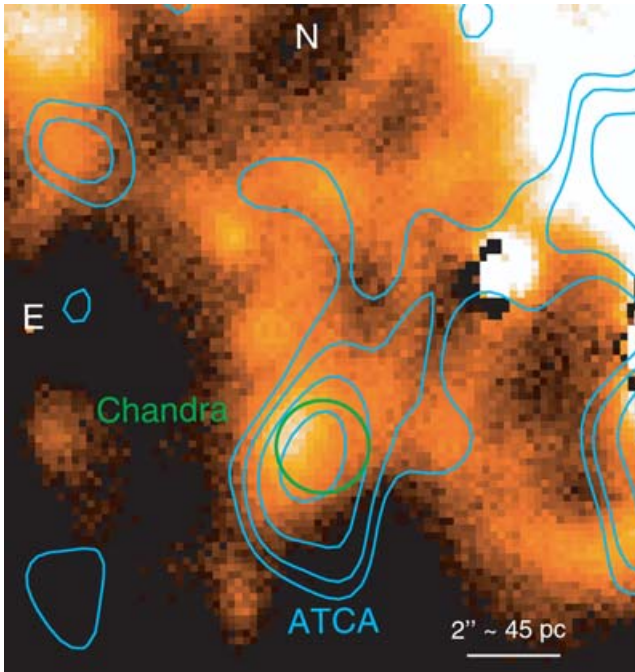


Figure 7. Close-up view of the region around X-1, in the continuum-subtracted $H\alpha$ image from the ESO 3.6-m telescope. A circle (green in the on-line version) marks the *Chandra* position; its 1-arcsec radius combines the rms error in the astrometric solution for the optical image with the astrometric uncertainty in the *Chandra* position. The ATCA 4.8-GHz radio flux density contours are overplotted (cyan, in the on-line version): the contours are for fluxes of 0.054, 0.081, 0.12 and 0.18 mJy beam⁻¹.

We stress that this $H\alpha$ nebula is not at all unique or remarkable for this galaxy, and is fainter than many other knots and filaments (Fig. 6), which are probably due to OB photoionization or local density enhancements in the outflowing warm gas. It is only its association with strong X-ray and synchrotron radio emission that makes it remarkable. Hence, we also need to consider the possibility that the local enhancement in the $H\alpha$ emission is directly caused by the ULX. We used *sc xspec* to re-analyse the *XMM-Newton* X-ray spectra of the ULX from 2001–2003 (Soria et al. 2004), using variable-abundance, ionized absorbers in addition to the Galactic line-of-sight term. We found that intrinsic absorption (column density $\approx 1 \times 10^{21}$ cm⁻²) removes $\approx 1.7 \times 10^{48}$ photons s⁻¹ with energies above 13.6 eV, assuming a thermal Comptonization model (bmc) for the X-ray spectrum.⁴ Plausible local interstellar gas densities $n_H \sim$ a few cm⁻³ are consistent with a significant fraction of the intrinsic absorption coming from $\lesssim 30$ pc from the ULX. Hence, photoionization from the ULX may contribute a similar amount of H-ionizing photons as the few OB stars in the surrounding region.

Finally, part of the $H\alpha$ emission may be due to shock ionization from an SNR. Most identified radio SNRs in nearby galaxies are associated with much brighter $H\alpha$ emission, from \sim a few 10^{-15} erg s⁻¹ cm⁻² up to \sim a few 10^{-14} erg s⁻¹ cm⁻² at the distance of X-1 (Deharveng et al. 1988; Hyman et al. 2000; Pannuti et al. 2000). This is partly due to a selection bias (e.g. Pannuti

⁴ Power-law plus blackbody models also provide good fits to the X-ray spectrum, but are less suitable for an extrapolation to the UV region, since they give unphysically high fluxes, unless the power-law component is truncated at low energies.

et al. 2000): unresolved, non-thermal (steep-spectrum) radio sources without optical line emission would generally be discarded as background active galactic nucleus (AGN). However, radio synchrotron and $H\alpha$ emission in SNRs come from different processes, and are not strongly correlated; in fact, there are a few radio-bright candidate SNR in nearby galaxies, with $H\alpha$ emission below the level inferred for the source in NGC 5408: for example, some sources in the Large Magellanic Cloud (LMC) (fig. 1a in Filipović et al. 1998).⁵ Other examples of $H\alpha$ -faint SNRs are found in NGC 300 (table 4 in Payne et al. 2004).

In summary, we conclude that the SNR scenario for the radio synchrotron emission remains viable, although probably not the most likely. We will also see in Section 3.6 that the radio source would require an explosion energy unusually high for a normal SN. In the optical band, more narrow-band imaging and spectral studies are needed to distinguish between the main competing scenarios (H II region, X-ray ionized nebula and shock-ionized SNR). Specifically, the most important constraints will come from the presence or absence of nebular [O III] and He II emission, and from the [S II]/ $H\alpha$ and [O I]/ $H\alpha$ line ratios.

3.6 Radio lobes?

Finally, we consider the possibility that the optically thin synchrotron radio emission comes from extended radio lobes associated with the ULX. While core emission from a radio jet (Sections 3.1–3.3) traces the instantaneous accretion power and spectral state of the BH, emission from radio lobes depends on the accretion activity integrated over the source lifetime (e.g. Scheuer 1974), even if the core were not currently active. Hence, we do not expect significant variability over a few years, in agreement with the observations.

Almost all radio-loud AGN show a lobe structure, which dominates the radio emission in Fanaroff–Riley type II (FR II) sources. On the other hand, while most X-ray binaries are thought to release part of their accretion power in a jet, only a few sources have been found so far with persistent lobe-like emission: Cyg X-1 (Gallo et al. 2005); Cir X-1 (Tudose et al. 2006); the Galactic microquasars 1E 1740.7–2942 and GRS 1758–258 (Mirabel et al. 1992; Hardcastle 2005). In addition, in SS 433, a radio-lobe structure may coexist with an underlying SNR (Downes, Pauls & Salter 1986; Dubner et al. 1998); it has been noted that SS 433 may be classified as a ULX if we could see it face-on (Fabrika & Mescheryakov 2001). The size of the steep-spectrum radio-lobe structure in SS 433 is $\approx (50 \times 100)$ ($d/3$ kpc) pc, very similar to the source in NGC 5408; however, the radio luminosity density is an order of magnitude lower.

The main difference between radio galaxy and microquasar lobes is due to the environment: while some quantities, such as all characteristic time-scales, length-scales and energies, scale as M_{BH} , others, such as the density of the ambient medium, do not (e.g. Heinz 2002). In particular, radio lobes in stellar-mass microquasars tend to be much more overpressured with respect to the external medium; therefore, they have a shorter lifetime due to adiabatic expansion (Hardcastle & Worrall 2000; Hardcastle 2005). None the less, Pakull & Mirioni (2002) discovered that many ULXs are indeed

⁵ For comparison with the plot in Filipović et al. (1998), the $H\alpha$ flux and 4.8-GHz radio flux density from the source in NGC 5408 would be $\approx 5 \times 10^{-12}$ erg cm⁻² s⁻¹ and ≈ 2.5 Jy, respectively, translated to the distance of the LMC.

surrounded by large optical nebulae possibly powered by the interaction of a jet with the ISM.

The spectral index and total radio power alone do not give us enough information to determine the physical parameters of the lobes – in particular, the energy density of the particles and the magnetic field. However, if the size of the lobes (hence, their surface brightness) is known, one can minimize the total energy density to get a rough constraint on the particle and field energy and pressure (e.g. Pacholczyk 1970). In our case, the radio source may be marginally resolved (Section 2), although its detailed spatial geometry is unknown. For simplicity, we take a spherical lobe with a radius of 30 pc (≈ 1.3 arcsec), a power-law distribution of relativistic electrons with spectral index -3 (corresponding to $\alpha_R = -1$), and we assume that the electron distribution extends between the Lorentz factors of 1 and 10^4 .⁶ We also assume a magnetic field randomly distributed with respect to the line of sight, and a volume filling factor ≈ 1 . See Appendix A for a brief summary of the formulae we used to estimate the minimum-energy magnetic field.

The matter content of a quasar or microquasar jet is still a hotly debated issue (Romero 2005). For example, the Galactic microquasar LS 5039 has been variously modelled with leptonic (Bosch-Ramon et al. 2005; Dermer & Böttcher 2006) or hadronic jets (Romero et al. 2003; Aharonian et al. 2005). An electron–positron plasma was suggested for the jet in Nova Muscae (GRS 1124–684) (Kaiser & Hannikainen 2002). On the other hand, a significant hadronic contribution could explain why synchrotron emission is not detected within the free–free emitting bubble of Cyg X-1 (Gallo et al. 2005). Hadronic jet models are also favoured for the microquasars SS 433 (Migliari, Fender & Mendez 2002), and LS I+61 303 (Romero, Christiansen & Orellana 2005). A leptonic model was instead suggested for the powerful quasar 3C 279 (Wardle et al. 1998), based on the detection of circular polarization.

From the observed 4.8-GHz flux, for an electron–positron plasma, we obtain: a minimum energy density $\approx 9.4 \times 10^{-10}$ erg cm⁻³ for a random magnetic field $B \approx 0.11$ mG;⁷ a minimum pressure $P_{in} \approx 5.4 \times 10^{-10}$ dynes cm⁻²; and a total energy $\approx 3.3 \times 10^{51}$ erg. Alternatively, taking two lobes with radii of 23 pc = 1 arcsec, the minimum pressure is $\approx 6.2 \times 10^{-10}$ dynes cm⁻² and the total energy is $\approx 2 \times 1.7 \times 10^{51}$ erg. Most quantities depend strongly on the adopted value of α_R . Taking $\alpha_R = -0.7$ as a strong upper limit, we infer a total energy $> 3.5 \times 10^{50}$ erg for a single 30-pc electron–positron bubble, or $> 3.6 \times 10^{50}$ erg for two 23-pc lobes.

If energy and pressure in the synchrotron-emitting bubble are dominated by relativistic protons, the total energy can be up to a factor of 10 higher than in the leptonic case, for the same sets of parameters. For example, if hadrons carry ~ 99 per cent of the energy,⁸ the minimum-energy condition implies a magnetic field $B \approx$

0.35 mG and a total energy $\approx 3.3 \times 10^{52}$ erg for a 30-pc synchrotron bubble with a spectral index $\alpha_R = -1$; our limit $\alpha_R < -0.7$ implies an energy $> 4.3 \times 10^{51}$ erg. Hence, the leptonic-jet assumption can be used as a conservative lower limit to the energy in the bubble.

On the other hand, relativistic hadrons do carry most of the energy in SNRs (known sources of cosmic rays). Therefore, if the radio source in NGC 5408 is interpreted as an SNR, we need to use the higher range of energy estimates. Energies $\sim 10^{52}$ erg are implausibly high for a single ‘standard’ SN. Following this argument leads us to conclude that an SNR interpretation is less likely than a radio-lobe scenario, but we cannot rule out the possibility of a more energetic hypernova remnant. Conversely, we could assume that the source is an SNR with a standard energy $\approx 10^{51}$ erg, and infer its size from the minimum-energy condition. It turns out that the remnant should be ≈ 10 – 15 pc in radius, for the observed flux and spectral index. Hence, deeper high-frequency radio observations will be crucial to unequivocally determine the size of the radio source (or at least a more stringent upper limit) and test the SNR scenario.

One might suggest that the injection spectral index was flatter ($\alpha_R \approx -0.5$), and the steeper index currently observed at high frequencies may simply be due to an ageing population of relativistic electrons inside the expanding bubble (‘spectral ageing’), as the higher energy electron population is depleted by synchrotron losses. If this is the case, the total energy in a 30-pc bubble would be lower, $\approx 1 \times 10^{51}$ erg (corresponding to a magnetic field $B \approx 0.07$ mG), consistent with a normal SN. The presence of a spectral break in the radio continuum would, in principle, provide another criterion to distinguish between an SNR and a jet-inflated lobe. For an SNR, we expect an exponential cut-off in the spectrum above the break frequency ν_{br} (Jaffe & Perola 1973); for a jet bubble, characterized by continuous injection, the spectrum would be a broken power law with an index $\alpha_R' = \alpha_R - 0.5$ above the break frequency (Kardashev 1962).

The problem with the spectral break scenario is that a relatively old age is required for the break to occur at frequencies as low as ~ 3 – 4 GHz. Following Murgia (2003), and using the previous order-of-magnitude estimate of the magnetic field, we obtain a characteristic age $\approx 8 \times 10^5 (B/0.1 \text{ mG})^{-1.5} (\nu_{br}/4 \text{ GHz})^{-0.5}$ yr for an expanding 30-pc bubble. SNRs of that age are unlikely to be still so bright. This age is also longer than the characteristic age we will estimate for the radio-lobe scenario (Section 4). However, even in this case, we cannot entirely rule out the break scenario, for example, if B is well above equipartition in a magnetically dominated outflow.

4 SELF-SIMILAR SOLUTION FOR RADIO LOBES

In Section 3.6, we have treated the size of the bubble simply as an arbitrary input parameter. We can learn more about the time-evolution of a jet-inflated bubble if we express its radius self-consistently as a function of the total energy injected into it, thus coupling a radial expansion equation with the energy density equation. To do so, we describe the supersonic (but subrelativistic) expansion and radio emission from the bubble with a set of self-similar solutions (Castor, McCray & Weaver 1975; Falle 1991), often adopted to model radio lobes in AGN and Galactic micro-quasars (Heinz, Reynolds & Begelman 1998; Willott et al. 1999; Jarvis et al. 2001; Heinz 2002). We assume (Heinz et al. 1998): a spherical, uniform radio cocoon of radius r_c ; a constant density of the external ISM

⁶ For a random magnetic field ≈ 0.1 mG, the synchrotron cooling time-scale of relativistic electrons is $\approx 10^5 \times (10^4/\gamma)$ yr, where γ is the Lorentz factor. Taking instead an upper limit $\gamma \sim 10^3$ for the electron distribution does not significantly affect our results: for our rather steep spectral index ≈ -1 , the minimum energy depends more strongly on the low-energy cut-off of the electron distribution. For example, a lower cut-off at $\gamma \sim 10$ would reduce the estimated energies by a factor of 3.

⁷ For the adopted spectral index $\alpha_R = -1$, the minimum-energy condition also implies energy equipartition, while for a spectral index $= -0.7$, the energy density of the magnetic field would be ≈ 85 per cent of the particle energy density.

⁸ a value typical of plasmas where electrons and positrons originate as secondary particles following collisions of a primary hadronic jet with the ISM (Pacholczyk 1970).

(an approximation suitable to microquasar environments); relativistic gas inside the radio bubble (adiabatic index = 4/3); non-relativistic gas in the shell outside the contact discontinuity (adiabatic index = 5/3); equipartition of field and particle energies in the cocoon; non-radiative shocks; a radio spectral index $\alpha_R = -1$. For simplicity, we use a density $\rho = 1.7 \times 10^{-27} n_H$, valid for a pure hydrogen gas; in any case, the main results from the self-similar solutions do not have a strong dependence on the mean atomic weight.

The self-similar equations governing the expansion of the bubble are (e.g. Heinz et al. 1998):

$$r_c \simeq 4.02 \times 10^4 n_H^{-1/5} \mathcal{L}^{1/5} t^{3/5} \quad (3)$$

and

$$\mathcal{L}t \equiv E_{\text{tot}}, \quad (4)$$

where E_{tot} is the total energy injected by the jet into the radio cocoon, and \mathcal{L} is the time-averaged jet power, assuming that it is either approximately constant, or with a duty cycle much shorter than the time t . The emitted flux density at a frequency ν is then

$$F_\nu = 0.41 \left(\frac{n_H}{\text{cm}^{-3}} \right)^{0.6} \left(\frac{\mathcal{L}}{10^{39} \text{ erg s}^{-1}} \right)^{1.4} \left(\frac{t}{10^5 \text{ yr}} \right)^{0.2} \times \left(\frac{\nu}{5 \text{ GHz}} \right)^{-1} \left(\frac{d}{4.8 \text{ Mpc}} \right)^{-2} \text{ mJy}. \quad (5)$$

See Appendix B for an outline of the derivation of equation (5).

We followed Willott et al. (1999) to obtain the normalization of the relations between jet power and age and radio flux of the cocoon (equations 3 and 5).⁹ The normalization factors are based on the estimated ages, ambient gas densities and 151-MHz flux densities for the FR II radio galaxies in the 7C Redshift survey. They also depend on the adopted value of a scaling factor f (as defined in Willott et al. 1999) for the total energy inside the cocoon, inferred from the minimum-energy condition. The factor f parametrizes our ignorance of the exact geometry of the cocoon, low-energy cut-off in the electron distribution, filling factor, deviations from equipartition and proton contribution. The assumptions we adopted in Section 3.6 to estimate the total energy correspond to a choice of $f \approx 15$, which is a plausible number for quasi-stellar object (QSO) radio lobes; it was estimated in Blundell & Rawlings (2000) that f is most likely to vary between ~ 10 and 20. Therefore, our normalization coincides with the one adopted by Punsly (2005), that is $\mathcal{L} = 4.0 \times 10^{46} \text{ erg s}^{-1}$ for $d^2 F_{151} = 10^{35} \text{ erg s}^{-1} \text{ Hz}^{-1} \text{ sr}^{-1}$. This choice of normalization may easily vary by a factor of 2 at the reference flux, and larger uncertainties may be introduced as we scale the solution from the parameter range suitable for radio-loud QSOs (e.g. $n_H \sim 10^{-3} \text{ cm}^{-3}$, $t \sim 10^7 \text{ yr}$ and $\mathcal{L} \sim 10^{46} \text{ erg s}^{-1}$), to the range suitable for microquasars (e.g. $n_H \sim 1 \text{ cm}^{-3}$, $t \sim 10^5 \text{ yr}$, $\mathcal{L} \lesssim 10^{39} \text{ erg s}^{-1}$). Another caveat is that sources with a radio spectral index ≈ -1 are outliers in the FR II sample: most have indices between ≈ -0.5 and ≈ -0.9 (e.g. fig. 5 in Willott et al. 1999).

Inserting the observed flux (0.28 mJy at 4.85 GHz) and speculative size ($r_c \approx 30 \text{ pc}$) of the radio-emitting bubble into equations (3)–(5), for an electron–positron plasma, we obtain an age $t \approx 1.43 \times 10^5 n_H^{1/2} \text{ yr}$, an average jet power $\mathcal{L} = 7.1 \times 10^{38} n_H^{-1/2} \text{ erg s}^{-1}$, a total energy $E_{\text{tot}} \approx 3.2 \times 10^{51} \text{ erg}$, and an expansion velocity $v \approx (2r_c/5t) \approx 82 n_H^{-1/2} \text{ km s}^{-1}$ at present time. We recall that we estimated (Section 3.6) a total pressure $P_{\text{in}} \approx 5 \times 10^{-10} \text{ dynes cm}^{-2}$

inside the lobes; this is much larger than the thermal pressure of the undisturbed ISM, which is $P_{\text{out}} \approx 3 \times 10^{-12} (n_H/1 \text{ cm}^{-3}) (T/10^4 \text{ K}) \text{ dynes cm}^{-2}$, with a sound speed $\approx 15 \text{ km s}^{-1}$ for $T \approx 10^4 \text{ K}$. The expansion of the bubble into the ISM is supersonic, with Mach number $\mathcal{M} \approx 82/15 \approx 5.5$. Hence, we expect the expanding cocoon to drive a strong shock into the ISM. Pressure balance should occur between the pressure inside the cocoon (P_{in}) and the thermal plus ram pressure of the shocked ambient gas, swept up in a shell outside the cocoon. Applying standard Rankine–Hugoniot conditions (e.g. Spitzer 1978), we expect a thermal pressure in the shocked gas $P_s = (5\mathcal{M}^2 - 1)P_{\text{out}}/4 \approx 37n_H^{-1}P_{\text{out}} \approx 1 \times 10^{-10} \text{ dynes cm}^{-2}$, a density of the shocked gas $\rho_s \approx 3.6$ times the ambient ISM density, and a ram pressure $\approx \rho_s v^2 \approx 4 \times 10^{-10} \text{ dynes cm}^{-2}$. Thus, even though our simple spherical model is only a crude approximation of a real radio lobe, we obtain that the total pressure inside the cocoon is balanced by the thermal plus ram pressure of the swept-up ISM, as we should expect.

A higher jet power and shorter bubble age are inferred if protons contribute a significant fraction of energy. For example, in the case of a 99 per cent hadronic contribution, we obtain an age $t \approx 5 \times 10^4 n_H^{1/2} \text{ yr}$, an average jet power $\mathcal{L} = 2 \times 10^{40} n_H^{-1/2} \text{ erg s}^{-1}$ and an expansion velocity $v \approx 230 n_H^{-1/2} \text{ km s}^{-1}$ at present time. The total energies and pressure inside the bubble are an order of magnitude higher than in the leptonic case ($\sim B^2$). The internal pressure is still roughly balanced by ram plus thermal pressure in the shocked gas ($\sim v^2$).

Finally, from the Rankine–Hugoniot equations we also predict a temperature in the swept-out shell ≈ 10 times the ambient ISM temperature, that is, $\approx 10^5 \text{ K}$. The shell thickness should be $\approx 0.1 r_c \approx 3 \text{ pc}$. We infer a cooling time-scale for the shocked gas $\approx 10^6 \text{ yr}$, that is, longer than the estimated lifetime of the radio cocoon. This may explain why we do not see stronger Balmer line emission from that region. The total synchrotron energy radiated over the lifetime of the bubble is also negligible [$O(10^{-2})$] compared with the injected energy $\mathcal{L}t$ (Willott et al. 1999). This explains why the value of E_{tot} in equation (4) can be treated as the total energy inside the bubble at present time.

Considering the various sources of uncertainty mentioned earlier, the scenario outlined in this section can only represent one possible solution in agreement with the (few) observed parameters. None the less, it is a plausible scenario, consistent with existing models for microquasars. As already mentioned in Section 3.1, a steady radio jet is thought to dominate the power output in the LHS, and a transient jet may be present in the VHS, while it is suppressed in the HS. In the conventional definition of LHS, the X-ray luminosity $L_X \lesssim 10^{-2} L_{\text{Edd}}$, and the jet power $L_J/L_{\text{Edd}} \approx A(L_X/L_{\text{Edd}})^{1/2}$, with $6 \times 10^{-3} \lesssim A \lesssim 0.3$ (Fender, Gallo & Jonker 2003; Fender et al. 2004; Malzac, Merloni & Fabian 2004). Hence, the jet power in the LHS is $L_J \lesssim 0.03 L_{\text{Edd}}$. We compare this value with the value of $\mathcal{L} \approx 7 \times 10^{38} \text{ erg s}^{-1}$ inferred from our self-similar solutions. If most of the energy has been injected into the bubble by a steady LHS jet over the past $\sim 10^5 \text{ yr}$, the Eddington luminosity has to be $\gtrsim 2 \times 10^{40} \text{ erg s}^{-1}$, corresponding to a BH mass $\gtrsim 150 M_\odot$. However, the upper limit to the luminosity in the LHS is somewhat conventional: a steady jet may persist (with a similar scaling) as the source moves up in luminosity into the ‘hard’ VHS, at $L_X \approx L_{\text{Edd}}$ (Fender et al. 2004). If the source spent most of its time in that state, $L_{\text{Edd}} \sim$ a few $10^{39} \text{ erg s}^{-1}$ would suffice. Finally, transient ejections with $L_J \sim 0.1\text{--}1 L_{\text{Edd}}$ occur at the spectral transition between ‘hard’ and ‘soft’ VHS.

We do not know how much time the X-ray source has spent in the different accretion states, and for what fraction of time it has been

⁹ A similar method was followed by Heinz (2002), see his equation (3), but with the assumption of a radio spectral index $\alpha_R = -0.5$, definitely ruled out in our case.

off. As we discussed in Section 3 (see also Soria et al. 2004), it is currently in some kind of VHS, with $L_X \approx 10^{40} \text{ erg s}^{-1}$ and some ongoing flaring activity suggesting coronal ejections. The estimated average jet power is at least consistent with a BH mass $\approx 100 M_\odot$. For comparison, GRS 1915+105 ($M_{\text{BH}} \approx 14 M_\odot$) spends long periods of time in a flaring state with $L_J \approx 10^{38} \text{ erg s}^{-1}$ and $L_X \approx 10^{39} \text{ erg s}^{-1}$ (Fender et al. 1999). The average jet power in SS 433 is thought to be $\sim 10^{39} \text{ erg s}^{-1}$ (Fabrika 2004, and references therein). In the ULX class, a jet power $\approx 1.5 \times 10^{39} \text{ erg s}^{-1} \approx 0.2 L_X$ would be required to explain the ionized bubble around NGC 1313 X-2 (Pakull & Mirioni 2002). Another example – at the opposite end of the BH mass range – is the quasar PKS 0743–67, showing a radio jet with $L_J \sim 0.1 L_{\text{Edd}} \sim 10^{46} \text{ erg s}^{-1}$ as well as an accretion luminosity $\sim L_{\text{Edd}}$ (Punsly & Tingay 2005).

5 CONCLUSIONS

We have used the ATCA to study the radio counterpart of a bright ULX in the starburst irregular galaxy NGC 5408. The spectrum is rather steep (single power-law index ≈ -1), typical of optically thin synchrotron. The flux has remained unchanged between 2000 March and 2004 December. We speculate that the source is marginally resolved in a composite (4.8 + 6.2)-GHz map, implying a size $\approx 50 \times 70 \text{ pc}^2$. However, deeper 6.2- or 8.4-GHz observations will be necessary to verify this hypothesis unequivocally, and to measure the spectral index more precisely.

We have discussed the possibility that the source represents the core radio emission from a ULX jet, as previously hypothesized (Kaaret et al. 2003). We argued that a steady jet in the LHS is inconsistent with its steep radio spectrum, its very high flux ($\approx 0.28 \text{ mJy}$ at 4.8 GHz) and the X-ray spectral and timing properties of the ULX. Therefore, simple BH mass determinations based on Fundamental Plane relations between LHS core radio and X-ray luminosities are not applicable to this object. A sporadic, major radio outburst is also ruled out, given the constant radio flux between the two epochs of the ATCA observations (2000 and 2004), and the X-ray behaviour. Radio emission from a persistent, flaring VHS (perhaps similar to the dip-flare state in GRS 1915+105, characterized by a sequence of repeated, minor ejections) can be consistent with the observed flux, if enhanced by (moderate) relativistic Doppler boosting. We consider this scenario slightly contrived, because there are currently no known examples of similar, persistent VHS flaring in Galactic microquasars. On the other hand, if the accreting BH has a mass $\sim 100 M_\odot$ as suggested by the X-ray luminosity (from the Eddington argument), the spectral-state transition pattern may be rather different from Galactic microquasars. The other reason why we consider core radio emission an unlikely scenario is that we have at least speculative evidence of a spatially resolved source.

Instead, we suggest that the emission could be either from an underlying SNR (perhaps related to the formation of the compact object powering the ULX), or from radio lobes inflated by a relativistic jet from the ULX. A young shell-like radio SNR could reach sufficient luminosity, would have a constant flux over many years, and has an optically thin synchrotron spectrum. However, in contrast with its unusually high radio luminosity, this source is extremely faint in the optical. From a continuum-subtracted $H\alpha$ image, one can see an H II region approximately coincident with the X-ray and radio sources. This region appears as a bright knot in a complex web of $H\alpha$ -emitting filaments, connected to the main starburst complex. We estimate a luminosity $\approx 1.5 \times 10^{36} \text{ erg s}^{-1}$ in the line. This is an upper limit to any possible contribution from an SNR. In fact, we showed that the few OB stars clearly detected

in the same region, and/or the X-ray source itself would contribute enough ionizing photons to explain the $H\alpha$ emission. A study of higher ionization lines will be required to determine the ionization mechanism. Moreover, if we accept the evidence for a marginally resolved radio source, standard equipartition arguments imply a total energy \gtrsim a few $\times 10^{51} \text{ erg}$, and probably as high as $\sim 10^{52} \text{ erg}$ in the SNR: this is extremely high for a single SN, and may require a hypernova or a few normal SNe going off in the same group of stars. We conclude that the SNR interpretation is unlikely, though not ruled out.

A radio lobe powered by a jet is thus the most likely scenario, in our opinion. In equipartition, the total energy content is $\sim 10^{51} \text{ erg}$ for a leptonic jet, or up to an order of magnitude higher if there is a significant hadronic contribution. We modelled the lobe as a spherical bubble of radius 30 pc, and solved a set of self-similar equations – often used in the literature to model radio lobes in FR II quasars – to relate the bubble expansion with the energy input (i.e. the jet power) and the observed radio flux and spectral index. Assuming an electron–positron plasma, we obtain that an average jet power $\approx 7 \times 10^{38} \text{ erg s}^{-1}$ over a time-scale $\approx 1.4 \times 10^5 \text{ yr}$ would indeed produce a 30-pc cocoon with the observed radio brightness, a total energy content $\approx 3 \times 10^{51} \text{ erg}$, with a randomly oriented magnetic field $\approx 0.1 \text{ mG}$. Such a bubble expands into the ambient ISM with a present speed of $\approx 80 \text{ km s}^{-1}$, sweeping up a shell of shocked gas. The pressure inside the bubble ($\approx 5 \times 10^{-10} \text{ dynes cm}^{-2}$) is balanced by the thermal plus ram pressure of the gas in the swept-up shell. An age $\sim 10^5 \text{ yr}$ implies that the steepness of the spectrum around 5 GHz is from injection and cannot be due to ageing (unless the magnetic field is well above equipartition); the age is also shorter than the radiative cooling time-scale of the gas in the swept-up shell.

An average jet power $\approx 7 \times 10^{38} \text{ erg s}^{-1}$ is almost an order of magnitude higher than the jet power in the most X-ray luminous Galactic microquasar, GRS 1915+105, during its long-term VHS oscillation cycles. The corresponding X-ray source, NGC 5408 X-1, is itself almost an order of magnitude more luminous than GRS 1915+105. On the other hand, an average jet power $\sim 10^{39} \text{ erg s}^{-1}$ has been inferred for SS 433 and for the ULX NGC 1313 X-2, both of which exhibit an extended lobe structure. We briefly summarized the accretion states in which a jet may be produced, and the relation between jet power, X-ray luminosity and Eddington luminosity. Our results are consistent with a luminosity $L_X \approx L_{\text{Edd}} \approx 10^{40} \text{ erg s}^{-1}$ (BH mass $\approx 100 M_\odot$), and an average jet power $L_J \sim 0.1 L_X$; they also suggest that the ULX has been at least moderately active (accretion power $\gtrsim 10^{-2} L_{\text{Edd}}$) for most of the past 10^5 yr .

Understanding this radio source in NGC 5408 is crucial for constraining the nature of ULXs, their association with starburst environments, their process of accretion, and in particular the balance between radiative luminosity emitted by the accretion disc and mechanical luminosity carried the jet. Very few ULXs have a detected radio counterpart. Two ULXs in M 82 may have radio counterparts: one is probably a SNR, while the nature of the other one is still unclear (Körding, Colbert & Falcke 2005); however, the physical association between those sources and the nearby ULXs is still uncertain, given the density of sources in that region. The only other unambiguous ULX-radio source association is in Holmberg II (Miller, Mushotzky & Neff 2005). In that case, too, the spectrum is consistent with optically thin synchrotron, though less steep than in our case ($\alpha_R \approx -0.5$). The Holmberg II radio source is resolved (size $\approx 50 \text{ pc}$) and has a flux density $\approx 0.7 \text{ mJy}$ at 5 GHz (Miller et al. 2005), corresponding to $\approx 0.3 \text{ mJy}$ at the distance of NGC 5408; hence, the two sources may be very similar (the X-ray luminosity and spectral properties of the corresponding ULXs are also similar: Dewangan

et al. 2004; Soria et al. 2004). In that case, the pure SNR scenario appears inconsistent with the optical line spectrum; the most likely interpretation is that the synchrotron bubble is powered by the ULX jet (Miller et al. 2005).

Finally, should we expect to find many more microquasar lobes in nearby galaxies, perhaps misidentified as SNR? Taking NGC 5408 and Holmberg II as typical cases, such lobes would require a jet injection power $\gtrsim 10^{39}$ erg s $^{-1}$ over $\gtrsim 10^5$ yr, in order to be detected by existing radio surveys of nearby galaxies. If we assume that the jet power $L_J \sim L_X \lesssim L_{\text{Edd}}$, such systems should be associated with potential ULXs. In some cases, the X-ray source may not be currently active (or active at ULX level), yet there would still be a bright synchrotron radio source, formed by the integrated source activity over its lifetime. Therefore, finding the number ratio between microquasar lobes with or without a currently active ULX core could in principle provide a constraint on the average duty cycle of ULX microquasars. As an example, two bright radio sources, consistent with synchrotron bubbles with minimum energies $> 10^{52}$ erg (hence, candidate microquasar lobes or hypernovae) have recently been discovered in NGC 7424 (Soria et al. 2006). One is associated with a transient ULX, the other has no corresponding X-ray source, down to a completeness limit $\approx 3 \times 10^{37}$ erg s $^{-1}$. Thus, one could speculate that the ULX responsible for latter radio source is currently in the off state. Further discussion of these issues is beyond the scope of this paper.

ACKNOWLEDGMENTS

We thank Richard Hunstead and Ilana Klamer for their technical support at the ATCA telescope, above and beyond the call of duty. We are grateful to Manfred Pakull for drawing our attention to the existence of an H α -emitting nebula at the ULX position. We also thank Geoff Bicknell, Chris Copperwheat, Mark Cropper, Zdenka Kuncić, Jasmina Lazendić, Tom Pannuti and Doug Swartz for useful discussions and suggestions, and the anonymous referee for a number of improvements to our paper. RS acknowledges support from an OIF Marie Curie Fellowship.

REFERENCES

Aharonian F., Anchordoqui L. A., Khangulyan D., Montaruli T., 2005, preprint (astro-ph/0508658)
 Bicknell G. V., 2005, Lecture Notes on High Energy Astrophysics. Australian National University, Canberra, <http://www.mso.anu.edu.au/~geoff/HEA/HEA.html>
 Blundell K. M., Rawlings S., 2000, AJ, 119, 1111
 Bosch-Ramon V., Romero G. E., Paredes J. M., 2005, A&A, 429, 267
 Brocksopp C. et al., 2002, MNRAS, 331, 765
 Burbidge G. R., 1956, ApJ, 124, 416
 Castor J., McCray R., Weaver R., 1975, ApJ, 200, L107
 Chevallier L., Collin S., Dumont A.-M., Czerny B., Mouchet M., Gonçalves A. C., Goosmann R., 2006, A&A, in press (astro-ph/0510700)
 Crummy J., Fabian A. C., Gallo L., Ross R. R., 2006, MNRAS, 365, 1067
 Deharveng L., Caplan J., Lequeux J., Azzopardi M., Breysacher J., Tarenghi M., Westerlund B., 1988, A&AS, 73, 407
 Dermer C. D., Böttcher M., 2006, ApJ, in press (astro-ph/0512162)
 Dewangan G. C., Miyaji T., Griffiths R. E., Lehmann I., 2004, ApJ, 608, L57
 Dickel H. R., Harten R. H., Gull T. R., 1983, A&A, 125, 320
 Downes A. J. B., Pauls T., Salter C. J., 1986, MNRAS, 218, 393
 Dubner G. M., Holdaway M., Goss W. M., Mirabel I. F., 1998, AJ, 116, 1842
 Dunne B. C., Gruendl R. A., Chu Y.-H., 2000, AJ, 119, 1172
 Duric N., Gordon S. M., Goss W. M., Viallefond F., Lacey C., 1995, ApJ, 445, 173

Fabrika S., 2004, ASPRV, 12, 1
 Fabrika S., Mescheryakov A., 2001, in Schilizzi R. T., ed., Proc. IAU Symp. 205. Astron. Soc. Pac., San Francisco, p. 268
 Falcke H., Körding E., Markoff S., 2004, A&A, 414, 895
 Falle S. A. E. G., 1991, MNRAS, 250, 581
 Fender R. P., Belloni T. M., 2004, ARA&A, 42, 317
 Fender R. P., Southwell K., Tzioumis A. K., 1998, MNRAS, 298, 692
 Fender R. P., Garrington S. T., McKay D. J., Muxlow T. W. B., Pooley G. G., Spencer R. E., Stirling A. M., Waltman E. B., 1999, MNRAS, 304, 865
 Fender R. P., Gallo E., Jonker P. G., 2003, MNRAS, 343, L99
 Fender R. P., Belloni T. M., Gallo E., 2004, MNRAS, 355, 1105
 Feng H., Kaaret P., 2005, ApJ, 633, 1052
 Filipović M. D., Jones P. A., White G. L., Haynes R. F., 1998, PASA, 15, 128
 Fiorito R., Titarchuk L., 2004, ApJ, 614, L113
 Gallo E., Fender R. P., Pooley G. G., 2003, MNRAS, 344, 60
 Gallo E., Fender R., Kaiser C., Russell D., Morganti R., Oosterloo T., Heinz S., 2005, Nat, 436, 819
 Georganopoulos M., Kazanas D., 2003, ApJ, 589, L5
 Georganopoulos M., Aharonian F. A., Kirk J. G., 2002, A&A, 388, L25
 Gierliński M., Done C., 2004, MNRAS, 349, L7
 Hardcastle M. J., 2005, A&A, 434, 35
 Hardcastle M. J., Worrall D. M., 2000, MNRAS, 319, 562
 Heinz S., 2002, A&A, 388, L40
 Heinz S., Reynolds C. S., Begelman M. C., 1998, ApJ, 501, 126
 Hjellming R. M., Rupen M. P., 1995, Nat, 375, 464
 Hjellming R. M. et al., 2000, ApJ, 544, 977
 Hyman S. D., Lacey C. K., Weiler K. W., Van Dyk S. D., 2000, AJ, 119, 1711
 Hyman S. D., Calle D., Weiler K. W., Lacey C. K., Van Dyk S. D., Sramek R., 2001, ApJ, 551, 702
 Jaffe W. J., Perola G. C., 1973, A&A, 26, 423
 Jarvis M. J. et al., 2001, MNRAS, 326, 1563
 Kaaret P., Corbel S., Prestwich A. H., Zezas A., 2003, Sci, 299, 365
 Kaiser C. R., Hannikainen D. C., 2002, MNRAS, 330, 225
 Karachentsev I. D. et al., 2002, A&A, 385, 21
 Kardashev N. S., 1962, SvA, 6, 317
 King A. R., Pounds K. A., 2003, MNRAS, 345, 657
 Körding E., Falcke H., Markoff S., 2002, A&A, 382, L13
 Körding E., Colbert E., Falcke H., 2005, A&A, 436, 427
 Laming J. M., Titarchuk L., 2004, ApJ, 615, L121
 Lazendić J. S., Dickel J. R., Jones P. A., 2003, ApJ, 596, 287
 Longair M. S., 1994, High Energy Astrophysics. Cambridge Univ. Press, Cambridge
 McClintock J. E., Remillard R. A., 2003, in Lewin W. H. G., van der Klis M., eds, Compact Stellar X-ray Sources. Cambridge Univ. Press, Cambridge, preprint (astro-ph/0306213)
 Malzac J., Merloni A., Fabian A. C., 2004, MNRAS, 351, 253
 Markoff S., Nowak M., Corbel S., Fender R., Falcke H., 2003, A&A, 397, 645
 Merloni A., Heinz S., di Matteo T., 2003, MNRAS, 345, 1057
 Migliari S., Fender R., Mendez M., 2002, Sci, 297, 1673
 Miller J. M., Fabian A. C., Miller M. C., 2004, ApJ, 614, L117
 Miller N. A., Mushotzky R. F., Neff S. G., 2005, ApJ, 623, L109
 Mirabel I. F., Rodríguez L. F., Cordier B., Paul J., Lebrun F., 1992, Nat, 358, 215
 Mirioni L., 2003, PhD thesis, Observatoire de Strasbourg
 Murgia M., 2003, PASA, 20, 19
 Orosz J. A. et al., 2001, ApJ, 555, 489
 Osterbrock D. E., 1989, Astrophysics of Gaseous Nebulae and Active Galactic Nuclei. University of California Press, Berkeley, CA
 Pacholczyk A. G., 1970, Radio Astrophysics. Freeman & Co., San Francisco
 Pakull M. W., Angebault L. P., 1986, Nat, 322, 511
 Pakull M. W., Mirioni L., 2002, Proc. Symposium New Visions of the X-ray Universe in the XMM-Newton and Chandra Era. ESTEC, The Netherlands, preprint (astro-ph/0202488)

- Pakull M. W., Mirioni L., 2003, *RMxAC*, 15, 197
- Pannuti T. G., Duric N., Lacey C. K., Goss W. M., Hoopes C. G., Walterbos R. A. M., Magnor M. A., 2000, *ApJ*, 544, 780
- Pannuti T. G., Duric N., Lacey C. K., Ferguson A. M. N., Magnor M. A., Mendelowitz C., 2002, *ApJ*, 565, 966
- Payne J. L., Filipović M. D., Pannuti T. G., Jones P. A., Duric N., White G. L., Carpano, S., 2004, *A&A*, 425, 443
- Pohl M., 1993, *A&A*, 270, 91
- Punsly B., 2005, *ApJ*, 623, L9
- Punsly B., Tingay S. J., 2005, *ApJ*, 633, L89
- Reynoso E. M., Goss W. M., 2002, *ApJ*, 575, 871
- Romero G. E., 2005, *ChJAA*, 5, 110
- Romero G. E., Torres D. F., Kaufman-Bernadó M. M., Mirabel I. F., 2003, *A&A*, 410, L1
- Romero G. E., Christiansen H. R., Orellana M., 2005, *ApJ*, 632, 1093
- Sault R. J., Teuben P. J., Wright M. C. H., 1995, *ASPC*, 77, 433
- Schaerer D., de Koter A., 1997, *A&A*, 322, 598
- Scheuer P. A. G., 1974, *MNRAS*, 166, 513
- Shrader C. R., Titarchuk L., 1999, *ApJ*, 521, L21
- Soria R., Motch C., Read A. M., Stevens I. R., 2004, *A&A*, 423, 955
- Soria R., Cropper M., Pakull M., Mushotzky R., Wu K., 2005, *MNRAS*, 356, 12
- Soria R., Kuncic Z., Broderick J. W., Ryder S. D. 2006, *MNRAS*, submitted
- Spitzer L., 1978, *Physical Processes in the Interstellar Medium*. Wiley, New York
- Sternberg A., Hoffmann T. L., Pauldrach A. W. A., 2003, *ApJ*, 599, 1333
- Stevens I. R., Forbes D. A., Norris R. P., 2002, *MNRAS*, 335, 1079
- Strohmayr T. E., Mushotzky R. F., 2003, *ApJ*, 586, L61
- Tudose V., Fender R. P., Kaiser C. R., Tzioumis A. K., van der Klis M., Spencer R. 2006, *MNRAS*, submitted
- Wardle J. F. C., Homan D. C., Ojha R., Roberts, D. H., 1998, *Nat*, 395, 457
- Weiler K. W., Panagia N., 1978, *A&A*, 70, 419
- Willott C. J., Rawlings S., Blundell K. M., Lacy M., 1999, *MNRAS*, 309, 1017
- Wu K. et al., 2002, *ApJ*, 565, 1161
- Xu J.-W., Zhang X.-Z., Han J.-L., 2005, *ChJAA*, 5, 165

APPENDIX A: NOTES ON THE MINIMUM-ENERGY CONDITION

Two alternative formulations are used in the literature to estimate the minimum energy associated with a radio source (e.g. Tudose et al. 2006). One choice (e.g. Pohl 1993; Bicknell 2005), arguably the more physical, is to assume an energy range (γ_{\min} , γ_{\max}) for the relativistic electrons. In this framework, following Bicknell (2005), a useful way of expressing the minimum-energy magnetic field is

$$\begin{aligned}
 B_{\min} &= \frac{m_e}{e} \left[\frac{p+1}{2} (1+k) C_1^{-1}(p) \frac{c}{m_e} \right]^{2/(p+5)} \\
 &\times \left[h(p, \gamma_{\min}, \gamma_{\max}) \frac{I_v v^{-\alpha_R}}{2r_c} \right]^{2/(p+5)} \\
 &\approx 5.687 \times 10^8 \times (3.291 \times 10^{37})^{2/(p+5)} \\
 &\times \left[\frac{p+1}{2} (1+k) C_1^{-1}(p) h(p, \gamma_{\min}, \gamma_{\max}) \right]^{2/(p+5)} \\
 &\times \left[\left(\frac{I_v/2r_c}{\text{erg s}^{-1} \text{ cm}^{-3} \text{ Hz}^{-1} \text{ sr}^{-1}} \right) v^{-\alpha_R} \right]^{2/(p+5)} G, \quad (\text{A1})
 \end{aligned}$$

where the energy spectrum of the electrons is $N(E) dE \sim E^{-p} dE$, $\alpha_R \equiv (1-p)/2$, m_e and e are the electron mass and charge, c the speed of light, I_v the specific surface brightness (flux per angular beam area), $2r_c$ is the characteristic source diameter and k is the ratio between the energy of protons and electrons. We have assumed a

filling factor of 1, for simplicity. The functions are

$$h(p, \gamma_{\min}, \gamma_{\max}) = \frac{1}{p-2} [\gamma_{\min}^{(2-p)} - \gamma_{\max}^{(2-p)}], \quad (\text{A2})$$

$$\begin{aligned}
 C_1(p) &= \frac{3^{p/2}}{2^{(p+13)/2} \pi^{(p+2)/2}} \\
 &\times \frac{\Gamma\left(\frac{p}{4} + \frac{19}{12}\right) \Gamma\left(\frac{p}{4} - \frac{1}{12}\right) \Gamma\left(\frac{p}{4} + \frac{1}{4}\right)}{\Gamma\left(\frac{p}{4} + \frac{7}{4}\right)}, \quad (\text{A3})
 \end{aligned}$$

and $\Gamma(z)$ is the Gamma function. The corresponding total (minimum) energy density is (Bicknell 2005):

$$\begin{aligned}
 \epsilon_{\min} &= \epsilon_e + \epsilon_B = \left(\frac{4}{p+1} + 1 \right) \left(\frac{B_{\min}^2}{2\mu_0} \right) \\
 &\approx 3.98 \times 10^{-3} \left(\frac{5+p}{p+1} \right) \left(\frac{B_{\min}}{G} \right)^2 \text{ erg cm}^{-3} \quad (\text{A4})
 \end{aligned}$$

In our analysis, we adopted $\gamma_{\min} \sim 1$, $\gamma_{\max} \sim 10^4$. For a steep spectrum, the minimum energy depends only very weakly on the high-energy cut-off. As for the low-energy cut-off, there are theoretical arguments and observational evidence for the presence of low-energy electrons in a radio lobe (e.g. Blundell & Rawlings 2000, their section 11.1).

The alternative choice (e.g. Burbidge 1956; Pacholczyk 1970; Longair 1994; Willott et al. 1999) is to assume a frequency range (ν_{\min} , ν_{\max}) of the radio emission. In that case, the magnetic field for which the energy density is minimized is (Longair 1994):

$$\begin{aligned}
 B_{\min} &\approx 119.7 C_2(p)^{4/7} (1+k)^{2/7} \left(\frac{V}{\text{cm}^3} \right)^{-2/7} \\
 &\times \left(\frac{L_v}{\text{erg s}^{-1} \text{ Hz}^{-1}} \right)^{2/7} G, \quad (\text{A5})
 \end{aligned}$$

where V is the volume of the bubble, and we have assumed a unit filling factor. The functions are

$$\begin{aligned}
 C_1(p) &\approx 2.344 \times 10^{25} \frac{(7.413 \times 10^{-19})^{(2-p)}}{(1.253 \times 10^{37})^{(p-1)/2}} \\
 &\times \frac{[\nu_{\min}^{(2-p)/2} - \nu_{\max}^{(2-p)/2}] \nu^{(p-1)/2}}{a(p)(p-2)}, \quad (\text{A6})
 \end{aligned}$$

$$a(p) = \frac{\sqrt{\pi}}{2(p+1)} \frac{\Gamma\left(\frac{p}{4} + \frac{19}{12}\right) \Gamma\left(\frac{p}{4} - \frac{1}{12}\right) \Gamma\left(\frac{p}{4} + \frac{5}{4}\right)}{\Gamma\left(\frac{p}{4} + \frac{7}{4}\right)}, \quad (\text{A7})$$

and $\Gamma(z)$ is again the Gamma function. The minimum energy density is then (e.g. Tudose et al. 2006):

$$\begin{aligned}
 \epsilon_{\min} &\approx 1.33 \times 10^9 C_2(p)^{4/7} (1+k)^{4/7} \left(\frac{V}{\text{cm}^3} \right)^{-4/7} \\
 &\times \left(\frac{L_v}{\text{erg s}^{-1} \text{ Hz}^{-1}} \right)^{4/7} \text{ erg cm}^{-3}. \quad (\text{A8})
 \end{aligned}$$

The physical connection between the two formalisms is that for an electron of energy γ , the peak of its synchrotron emission is at a frequency

$$\nu \approx 0.29 \times \frac{3eB}{4\pi m_e} \gamma^2 \approx 1.22 \times 10^6 \left(\frac{B}{G} \right) \gamma^2 \text{ Hz}. \quad (\text{A9})$$

In some cases (e.g. Willott et al. 1999; Punsly 2005), the minimum-energy quantities are estimated for a conventional lower cut-off at

$\nu_{\min} = 10$ MHz (lowest frequency accessible to Earth-based radio observations), and then the energy density is corrected by a numerical factor $f > 1$ to account for low-energy electrons emitting below 10 MHz, and for hadronic contributions. In our case, setting a low-frequency limit of 10 MHz would imply an implausibly high $\gamma_{\min} \approx 300$ for a leptonic plasma. Empirically, it was shown (Blundell & Rawlings 2000; Punsly 2005) that the energy in the lobes of radio galaxies is ≈ 10 – 20 times the minimum energy estimated from a leptonic plasma with a 10-MHz cut-off. For a radio spectral index ≈ -1 , our choice of a leptonic plasma with $\gamma_{\min} \approx 1$, $\gamma_{\max} \approx 10^4$ corresponds to a correction factor $f \approx 15$, consistent with the observations (see also Section 4).

APPENDIX B: TIME-EVOLUTION OF THE RADIO BUBBLE

We outline here the derivation of equation (5) from equations (3) and (4) and the minimum-energy condition. Adopting Falle (1991)’s self-similar solution, the radius r_c of an expanding cocoon scales as:

$$r_c \propto \rho(r)^{-1/(5-\zeta)} \mathcal{L}^{1/(5-\zeta)} t^{3/(5-\zeta)}, \tag{B1}$$

where the density $\rho(r) \sim \rho_0 r^{-\zeta}$. For a constant ISM density ($\zeta = 0$),

equation (B1) reduces to equation (3). The bubble size is also related to the total energy $E_{\text{tot}} = V \epsilon_{\text{tot}} \sim r_c^3 \epsilon_{\text{tot}}$, and from equation (4):

$$1 r_c \propto \mathcal{L}^{1/3} t^{1/3} \epsilon_{\text{tot}}^{1/3}, \tag{B2}$$

In the minimum-energy approximation, $\epsilon_{\text{tot}} = \epsilon_{\min}$. Hence, from equations (A1) and (A5),

$$\epsilon_{\text{tot}} \propto r_c^{-12/(p+5)} \left[F_v d^2 v^{(p-1)/2} \right]^{4/(p+5)}. \tag{B3}$$

With simple algebraic manipulations, the system of equations (B1)–(B3) can be solved as:

$$F_v \propto \rho(r)^{\frac{3+3p}{4(5-\zeta)}} \mathcal{L}^{\frac{22-5\zeta+2p-p\zeta}{4(5-\zeta)}} t^{\frac{16-5\zeta-4p-p\zeta}{4(5-\zeta)}} v^{\frac{1-p}{2}} d^{-2}, \tag{B4}$$

which is identical to equation (5) for $\zeta = 0$ and $p = 3$. Similarly to Heinz (2002) (who discussed the case $p = 2$), the normalization coefficient in front of equation (B4) was fixed to be consistent with Willott et al. (1999)’s study of radio-lobe properties in radio galaxies (Section 4).

This paper has been typeset from a $\text{\TeX}/\text{\LaTeX}$ file prepared by the author.